

Structural Invariance of a Zn^{II} Coordination Polymer with 5-Aminoisophthalic Acid under Different Synthetic Conditions

Iara M. L. Rosa,^{*a} Ana C. Z. dos Santos,^a Luana A. R. Giusto,^a Carlos B. Pinheiro^b and Antonio C. Doriguetto^{*a}

^aLaboratório de Cristalografia, Instituto de Química, Universidade Federal de Alfenas, 37130-000 Alfenas-MG, Brazil

^bLaboratório de Cristalografia, Departamento de Física, Universidade Federal de Minas Gerais, 30161-970 Belo Horizonte-MG, Brazil

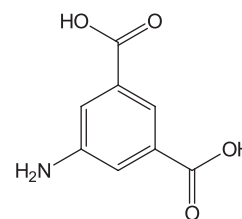
A same coordination polymer [Zn(aip)(DMSO)] (aip: 5-aminoisophthalate and DMSO: dimethylsulfoxide) was synthesized using the same reactants (ZnSO₄, aip and H₂O/DMSO) but in different conditions, in which the stoichiometry (1:1-4:1 metal:ligand ratio), temperature (70 and 100 °C) and synthetic method (liquid-liquid diffusion, solvothermal and conventional with stirring) varied. A liquid assisted mechanochemical approach using ZnO as Zn^{II} source instead ZnSO₄, but keeping DMSO as milling liquid, also resulted in the same compound. This new coordination polymer was investigated using single-crystal X-ray diffraction technique, revealing a two-dimensional honeycomb-type network formation. The crystal structure was compared with either similar or isostructural compounds reported in the literature. Our studies show that the synthetic method and other synthetic variables do not affect the formation of [Zn(aip)(DMSO)] coordination polymers and probe the high stability (thermodynamic and kinetic) and structural invariance of this structure.

Keywords: coordination polymer, zinc aminoisophthalate, network stability, X-ray diffraction

Introduction

The term coordination polymers (CPs) is used to describe a large and continuously growing class of polymeric compounds that comprise two parts: metal ions (inorganic) and ligands (in most cases, organic) linked by covalent bonds, which extend into one (1D), two (2D) or three (3D) dimensions.¹ Amino carboxylic acid derivatives as 5-aminoisophthalic acid (H₂aip or aip for its dianion species) (Scheme 1) are widely quoted in the literature as CP former.² Specifically, H₂aip has two carboxylate groups at the 1 and 3 positions that have been demonstrated as an excellent structure motif for constructing different secondary building unit (SBUs).³ In addition, the amino group may also affect the assembly process of CPs acting either as a new coordination site to bond with more metal centers or a hydrogen bond donor or acceptor to enhance the number of non-covalent interactions.⁴

The synthesis and structural characterization of CPs have continued to expand as areas of extremely active research



Scheme 1. Chemical structure of the 5-aminoisophthalic acid (H₂aip or aip in its deprotonated form).

in recent years.⁵ However, precise prediction or modulation of such materials with desired structures and properties remains an intimidating task.⁶ The relationship between the framework structure and the synthesis conditions is poorly understood.⁷ Although the crystal-growth and design of exact structures are still a great challenge, they can be achieved based on empirical observation and understanding of the construction of building blocks, which is known as rational design strategy.^{8,9}

The design of supramolecular materials can be governed by the careful choice of reaction conditions.¹⁰ The final results of the reagent mixture can be driven by subtle kinetic and thermodynamic details of the chemical and crystal

*e-mail: cristalografia.landre@gmail.com; doriguetto@unifal-mg.edu.br

growth processes.¹¹ Temperature and concentration, e.g., are important variables that influence the thermodynamics and kinetics of a chemical reaction and crystal growth, and consequently the obtained solid phases.¹² Almost all inner (such as coordination geometry, metal ions, structural characteristics of organic ligand and solvent system) and outer (such as temperature, concentration, stoichiometry and pH) synthetic factors have crucial effects on the formation and crystallization process^{13,14} and make CPs difficult to be exactly predicted and controllably synthesized.¹⁵ The influence of inner and outer factors on the CP products can be exemplified, e.g., respectively, by the four different 3D CPs of Mn^{II} with 6,6'-dinitro-2,2',4,4'-biphenyl tetracarboxylic acid obtained by solvothermal method varying the solvent system,¹⁶ and by the five different CPs of Zn^{II} with 4,4'-oxidiphthalic acid and 1,2-bis(4-pyridyl)ethane obtained by solvothermal method using a same solvent system but varying pH (acidity-controlled polymeric architecture construction).¹⁷

Besides inner and/or outer factors, the synthetic method itself may also guide the obtained product as previously highlighted by us working with Co^{II} and Zn^{II} and fumaric and 2,5-dihydroxyterephthalic acids reacted in water plus DMSO solvent mixture.¹⁴ The use of diffusion method favors the formation of 1D CPs,¹⁴ whereas the use of pH control method favors the formation of 3D CPs.^{14,18} It was demonstrated that the synthetic method could play a crucial role in the structure and dimensionality of CPs since the same starter reactants provided distinct products.¹⁴ Moreover, it was discussed that the obtained 1D (diffusion method) and 3D (pH control method) CPs were the thermodynamic and kinetics favored species, respectively.^{14,19}

Studies evidencing the influence of synthetic factors (inner and/or outer factors) have been also reported for CPs containing aip as linker. As examples, can be cited the two Co^{II} CPs (3D rutile-type *vs.* 2D (4,³₆) nets) obtained under solvothermal conditions varying solvent system (water *vs.* ethanol/water),²⁰ and the two Co^{II} CPs (both with 3D dimensionality but with different topologies) solvothermally obtained varying reactional temperature and solvent system.^{21,22}

On the other hand, there are reports showing that different synthetic methods can also drive to a same CP. We can quote the synthesis of CPs of Co^{II} and Cd^{II} with H₂aip, which were obtained by either diffusion²⁰ or solvothermal²³ methods, resulting in invariant structures (2D CP, with (4,³₆) topology) against the change of either metal ion or synthetic method. Another example showing the invariance of the topology against either synthetic method or solvent system involves Zn^{II} cation and H₂aip ligand. Three [Zn(aip)(L)] (where L: H₂O;²⁴ DEF: diethylformamide;²⁵ or

DMA: dimethylacetamide)²⁶ analogous present a same 6³ uninodal honeycomb-type network (hcb net) despite either the solvent completing the metal coordination sphere (H₂O, DEF or DMA) or the method (hydrothermal or conventional heating) used to prepare them.

Therefore, although in the past few decades, studies in this field have been focused on the elucidation of the role of these foregoing factors, the comprehensive effect of various influence factors on the formation of coordination polymers is less well understood and systematic studies are still rare.²⁷ Knowing that this difficulty of structural prediction can be seen with a branch of opportunity in obtaining interesting new structures, it also acts as a challenge for control in obtaining desired structures. Thus, this work aims to show the probe of influence of several synthetic factors in getting a Zn^{II} coordination polymer with H₂aip ([Zn(aip)(DMSO)] (**1**)) and the detailed structural study of this compound, comparing with analogues reported in literature.

Experimental

Materials and methods

The ligand used in this work (5-aminoisophthalic acid (94%)) was commercially distributed by Aldrich®, other reagents and chemicals were commercially purchased and used as received. Powder X-ray diffraction (PXRD) data were collected on an Empyrean PanAnalytical diffractometer with Cu K α radiation (λ at 1.5418 Å) in the angular range of 5–40° (2 θ). Thermogravimetric analyses were performed with an SDT Q600 (TA Instruments) unit at a heating rate of 10 °C min⁻¹ in a synthetic air atmosphere. The elemental analysis for C, H and N was performed using a LECO TruSpec Micro analyzer. The Fourier transform infrared spectroscopy (FTIR) analysis was conducted on a Shimadzu IRPrestige-21 spectrophotometer with 4 cm⁻¹ of resolution in the range of 4000–400 cm⁻¹ using KBr pellets.

Synthetic procedures

Synthesis of [Zn(aip)(DMSO)] (**1**)

Liquid-liquid diffusion method (method A)

A DMSO solution of H₂aip (0.25 mmol, 2 mL) at the bottom of a glass tube (13 × 100 mm) was covered with a DMSO/water mixture (3:1 v v⁻¹, 4 mL), over which an aqueous solution of metal salt ZnSO₄·7H₂O (1.00–0.25 mmol, 2 mL) was layered. The system was maintained at 30 °C. Additionally, in order to study the effect of the metal:ligand stoichiometry in the synthesis of **1**, the 1:1, 2:1, 3:1 and 4:1 (metal:ligand) stoichiometries were also compared. Over

a period of two months, the metal salt solution gradually diffused in the solvent mixture with concomitant formation of brown single crystals of the product on the vial walls. The obtained single crystals were separated and labeled as products **1a**, **1b**, **1c** and **1d** corresponding, respectively, to the glass tubes in which the 1:1, 2:1, 3:1 and 4:1 (metal:ligand) stoichiometries were tested.

Product **1a**

Elemental analysis (%) calcd. for $C_{10}H_{11}NO_5SZn$: C, 37.23; H, 3.44; N, 4.34%; found: C, 36.78; H, 3.51; N, 7.73; FTIR (KBr) ν_{max} / cm^{-1} 3442.94, 3253.91, 3136.25, 3072.60, 2995.45, 2914.44, 1701.22, 1629.85, 1587.42, 1575.84, 1483.26, 1440.83, 1392.61, 1348.24, 1319.31, 1251.80, 1190.08, 1134.14, 1109.07, 1028.06, 999.13, 966.34, 935.48, 894.97, 796.60, 777.31, 732.95, 677.01, 617.22, 570.93, 536.21, 459.06.

Product **1b**

Elemental analysis (%) calcd. as **1a**; found: C, 36.51; H, 3.34; N, 7.33; FTIR (KBr) ν_{max} / cm^{-1} 3442.94, 3253.91, 3136.25, 3068.75, 2993.52, 2914.44, 1701.22, 1627.92, 1589.34, 1573.91, 1479.40, 1440.83, 1394.83, 1348.24, 1321.24, 1251.80, 1190.08, 1132.36, 1111.00, 1028.06, 999.13, 964.41, 935.48, 898.93, 796.60, 775.38, 732.95, 677.01, 617.22, 572.86, 536.21, 459.06.

Product **1c**

Elemental analysis (%) calcd. as **1a**; found: C, 36.15; H, 3.46; N, 7.73; FTIR (KBr) ν_{max} / cm^{-1} 3442.94, 3257.77, 3134.33, 3068.75, 2995.45, 2914.44, 1701.22, 1624.06, 1589.34, 1573.91, 1481.33, 1440.83, 1409.83, 1350.17, 1321.24, 1251.86, 1190.08, 1126.43, 1112.93, 1028.06, 1001.06, 966.34, 935.48, 898.93, 800.46, 771.53, 738.74, 677.01, 617.22, 572.86, 538.14, 459.06.

Product **1d**

Elemental analysis (%) calcd. as **1a**; found: C, 36.15; H, 3.46; N, 7.73; FTIR (KBr) ν_{max} / cm^{-1} 3446.79, 3255.84, 3136.25, 3070.68, 2995.45, 2914.44, 1701.22, 1629.85, 1589.34, 1575.84, 1479.40, 1440.83, 1394.83, 1348.24, 1319.31, 1251.80, 1188.15, 1132.21, 1111.00, 1028.06, 999.13, 966.34, 935.48, 898.83, 796.60, 777.31, 732.95, 677.01, 617.22, 572.86, 538.14, 460.99.

Conventional synthesis with stirring (method B)

An aqueous solution (5 mL) of $ZnSO_4 \cdot 7H_2O$ (2.00 mmol) was added to a solution of H_2aip (1.00 mmol) in DMSO (15 mL). This mixture was adjusted to pH ca. 7 using a pH meter by addition of aqueous solution of NaOH (1.00 mol L⁻¹). The resulting solution was stirred for 24 h at

room temperature. The beige precipitate, labeled as product **1e**, was filtered, washed with water and dried in vacuum.

Product **1e**

Elemental analysis (%) calcd. as **1a**; found: C, 37.25; H, 3.52; N, 7.73; FTIR (KBr) ν_{max} / cm^{-1} 3442.94, 3253.91, 3136.25, 3068.75, 2993.52, 2914.44, 1701.22, 1627.92, 1589.34, 1573.91, 1479.40, 1440.83, 1394.83, 1348.24, 1321.24, 1251.80, 1190.08, 1132.36, 1111.00, 1028.06, 999.13, 964.41, 935.48, 898.93, 796.60, 775.38, 732.95, 677.01, 617.22, 572.86, 536.21, 459.06.

Solvothermal method (method C)

A mixture of $ZnSO_4 \cdot 7H_2O$ (2.00 mmol), H_2aip (1.00 mmol), water (5 mL) and DMSO (15 mL) was sealed in a 150 mL Teflon reactors and heated at 70 and 100 °C for 24 h. The beige precipitates obtained at 70 and 100 °C were respectively labeled as products **1f** and **1g**. The use of two different temperatures aimed to study its effect on the synthesis of **1**.

Product **1f**

Elemental analysis (%) calcd. as **1a**; found: C, 37.21; H, 3.76; N, 7.73; FTIR (KBr) ν_{max} / cm^{-1} 3446.79, 3251.98, 3138.18, 3070.68, 2993.52, 2915.75, 1701.22, 1627.92, 1591.27, 1573.91, 1477.47, 1440.83, 1392.61, 1346.31, 1321.24, 1251.80, 1190.08, 1134.14, 1111.00, 1099.43, 1028.06, 999.13, 966.34, 935.48, 925.83, 898.93, 796.60, 777.31, 732.95, 678.94, 617.22, 577.86, 538.14, 460.99.

Product **1g**

Elemental analysis (%) calcd. as **1a**; found: C, 37.25; H, 3.52; N, 7.73; FTIR (KBr) ν_{max} / cm^{-1} 3446.79, 3251.98, 3138.18, 3070.68, 2993.52, 2912.51, 1701.22, 1627.92, 1591.27, 1573.91, 1477.47, 1440.83, 1392.61, 1346.31, 1321.24, 1251.80, 1190.08, 1134.14, 1109.07, 1099.43, 1028.06, 999.13, 966.34, 935.48, 925.83, 898.93, 796.60, 777.31, 732.95, 678.94, 617.22, 572.86, 538.14, 460.99.

Liquid assisted mechanochemical method (method D)

ZnO (2.00 mmol) was milled with H_2aip (1.00 mmol) for 30 min in the presence of 1 mL of DMSO, which formed a beige grinded samples termed as product **1h**. No further purification/crystallization procedure was performed after milling process. Therefore, it is the only method among those used here that does not allow single crystal growth suitable for single crystal x-ray diffraction experiments.

Product **1h**

Elemental analysis (%) calcd. as **1a**; found: C, 29.63; H, 2.88; N, 3.92; FTIR (KBr) ν_{max} / cm^{-1} 3366.79, 3251.98,

3138.18, 3072.60, 2993.52, 2914.44, 1701.22, 1627.92, 1591.27, 1575.84, 1477.47, 1440.83, 1394.53, 1340.53, 1321.24, 1251.80, 1190.08, 1134.14, 1109.07, 1100.60, 1028.06, 999.13, 966.34, 935.48, 925.83, 893.04, 796.60, 779.24, 732.95, 678.94, 617.22, 577.86, 538.14, 459.06.

Single-crystal X-ray diffraction

The best single crystals of **1** suitable for single crystal X-ray diffraction experiment were obtained by liquid-liquid diffusion method (method A). The well-shaped chosen single crystal used for the X-ray diffraction data collection was arbitrary separated from the product **1a**. The X-ray diffraction measurement was performed on an Oxford Diffraction Gemini diffractometer using graphite-enhance source Mo K α radiation (λ at 0.71073 Å). Data integration and scaling of the reflections and analytical absorption corrections were performed with the programs of the CrysAlis suite.²⁸ The final unit cell parameters were based on the fitting of all reflection positions. The structures were solved by direct methods using the Sir-92 program.²⁹ The positions of the carbon, oxygen, sulfur, nitrogen and metal atoms were unambiguously assigned on consecutive difference Fourier maps. Refinements were performed with SHELXL³⁰ based on F² through a full-matrix least-square routine. All atoms except hydrogen were refined with anisotropic atomic displacement parameters. Hydrogen was located in difference maps and included as fixed contributions according to the riding model. For organic moieties, the constraints were C–H distance of 0.97 Å and $U_{\text{iso}}(\text{H}) = 1.5 U_{\text{eq}}(\text{C})$ for methyl groups, and C–H distance of 0.97 Å and $U_{\text{iso}}(\text{H}) = 1.2 U_{\text{eq}}(\text{C})$ for aromatic carbon and protonated nitrogen atoms. The crystal data and details of data collection and refinement are shown in Table 1.

Results and Discussion

Structural invariance of [Zn(aip)(DMSO)] (**1**) under different synthetic conditions

The starter reactants constituted by ZnSO₄ or ZnO as Zn^{II} source, H₂aip as ligand, and DMSO as solvent, were used here in a wide range of reaction conditions in order to investigate the influence of synthetic methods in the structure and dimensionality of CPs (Figure 1). In addition, two reactional outer factors (metal:ligand stoichiometry and temperature) were also studied (Figure 1).

Initially, the work aimed to verify the influence of two synthetic method (liquid-liquid diffusion vs. conventional) in the structure and dimensionality of CPs obtained from Zn^{II}, H₂aip and DMSO. The liquid-liquid diffusion

Table 1. Crystallographic data for compound **1**

Crystal data	
Chemical formula	C ₁₀ H ₁₁ NO ₃ SZn
M _r	322.63
Crystal system, space group	monoclinic, P2 ₁ /c
Temperature / K	150
a, b, c / Å	9.8569 (6), 7.6800 (4), 16.1298 (8)
β / degree	95.220 (5)
V / Å ³	1215.98 (11)
Z	4
Radiation type	MoK α
μ / mm ⁻¹	2.21
Crystal habit	plate
Crystal size / mm	0.28 × 0.20 × 0.12
Data collection	
No. of measured, independent and observed [$I > 2\sigma(I)$] reflections	10560, 3009 and 2265
R _{int}	0.049
$(\sin \theta/\lambda)_{\text{max}} / \text{\AA}^{-1}$	0.694
Refinement	
R[F ² > 2 σ (F ²)], wR(F ²) and S	0.044, 0.098 and 1.07
No. of reflections	3009
No. of parameters	164
No. of restraints	0
H-atom treatment	H atoms treated by a mixture of independent and constrained refinement
$\Delta\rho_{\text{max}}, \Delta\rho_{\text{min}} / (\text{e \AA}^{-3})$	0.98, -1.15
$w = 1/[\sigma^2(F_o^2) + (0.0274P)^2 + 2.7606P]$, where $P = (F_o^2 + 2F_c^2)/3$.	

(method A) and conventional (method B) methods were the initial choices in the expectation of obtaining different CPs as previously observed by us reacting Zn^{II} with fumarate (fum) or 2,5-dihydroxyterephthalate (dhbdc) in water-DMSO.¹⁴ The 2:1 metal:ligand ratio was the stoichiometry chosen to compare the influence of the methods in the expectation of obtaining higher dimensionality CPs (2D or 3D) as achieved by Dietzel *et al.*¹⁸ working with Zn^{II} and dhbdc. Indeed, in our previous work, the 2:1 metal:ligand stoichiometry of the starter reactants resulted in 1D CPs with 1:1 metal:ligand ratio using method A,¹⁴ and 3D CPs with 2:1 metal:ligand ratio using method B.^{14,18}

Contrary here, the same starter reactants, now having aip as ligand instead fum or dhbdc, result in a same product, characterized as [Zn(aip)(DMSO)] (**1**) (see single crystal X-ray results), regardless of whether the method is A or B (Figure 1). Therefore, establishing an analogy with our previous results,¹⁴ compound **1** can be considered both the kinetic and the thermodynamically stable product.¹⁹

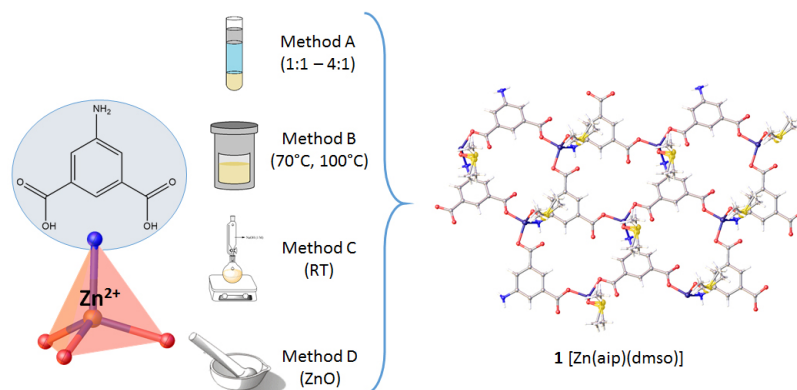


Figure 1. Representation of syntheses conducted in this work.

Interestingly, compound **1** was characterized as being a CP with a 1:1 metal:ligand ratio (see the bulk material characterization discussed below) but presenting a 2D dimensionality (see single crystal X-ray results).

After showing the invariance of the final product against methods A and B, we decided to probe this trend against to solvothermal (method C) and liquid assisted mechanochemical (method D) methods. Once again, compound **1** was the CP obtained, at least as majority crystal phase (see powder X-ray results), by varying the method but keeping (except to method D for which ZnO was used instead ZnSO₄) the starter reactants.

In sequence, since stoichiometry and temperature can also influence the thermodynamics and kinetics of a chemical reaction,¹² these outer reactional factors were also evaluated separately in two of the four synthetic method studied here. First, in addition to the 2:1 metal:ligand stoichiometry used to compare the four different methods, the 1:1, 3:1 and 4:1 stoichiometries were also tested in method A. Over again, the bulk materials obtained from all stoichiometries result in **1** as pure crystal phase (see powder X-ray results), even for the 3:1 and 4:1 metal:ligand stoichiometries, that could favor the formation of CPs with other structures or higher dimensionalities.^{14,18} Finally, since the use of temperature is an intrinsic variant in the hydrothermal via, this method was chosen to test the influence of this variable in the structure and dimensionality of the CPs obtained from the starter reactants used here. The tested reactional temperatures, 70 and 100 °C, results in bulk materials constituted by a mixture of compound **1** (majority phase) and a spurious unknown crystal phase (see PXRD discussion).

The experimental PXRD patterns of the products **1a-1h** (Figure 2) were obtained to evaluate both the formation of **1** and the crystalline purity of the bulk materials containing it. The calculated PXRD pattern of **1** was obtained from the CIF file of the single crystal X-ray diffraction data

reported here (see below) using the software Mercury.³¹ The 2θ positions and intensities of the calculated PXRD pattern of **1** do match those observed in the experimental PXRD patterns performed to the respective bulk material from the all tested synthetic methods (Figure 2), although the calculated and reported intensities of some reflections (mainly for **1a**) were slightly different because of preferred orientation effects on the powder sample analyzed. Therefore, by the analysis of the PXRD data, it can be verified that all methods and their variants (reactant stoichiometry or temperature) lead to compound **1**.

The phase purity was also confirmed for the products from methods A (**1a-1d**) and B (**1e**), since no evident spurious peak is observed in their experimental PXRD patterns (Figure 2a). On the other hand, for the products from methods C (**1f** and **1g**), the experimental PXRD patterns (Figure 2b) show the presence of extra Bragg peaks that do not match to the calculated ones for **1**. The spurious phase present in the bulk material of the products **1f** and **1g** is highlighted mainly by the peak at 2θ ca. 11.35° (Figure 2b). Unfortunately, attempts to identify this second crystal phase by search/match procedures were unsuccessful due to the presence of few peaks indexed to it. Therefore, in spite of compound **1** is the majority grown phase, it cannot be ruled out that method C may have led to a second CP of Zn^{II} and aif.

Peaks at 2θ equal to 31.74, 34.42 and 36.29°, which correspond to the Bragg peaks (100), (002) and (101) of the ZnO wurtzite structure (ICDD crystal chart No. 36-1451), are clearly observed in the PXRD pattern of the bulk material obtained from method D (**1h**) (Figure 2b). Actually, a physical mixture containing **1** and ZnO is expected due to the excess of ZnO (2:1 metal:ligand stoichiometry) used as source of Zn^{II} in the one-step liquid assisted mechanochemical method without post-purification. Indeed, the presence of ZnO as remaining reactant of designed CPs has been frequently observed, even in liquid

assisted grinding using 1:1 metal:ligand stoichiometry.³² Another detachable feature of the experimental PXRD pattern of the product **1h** is the noticeable broadening of the peaks attributed to compound **1** compared to the remaining experimental patterns. Actually, the broadening is expected due to the smaller crystallite size of this sample as consequence of the milling procedure.

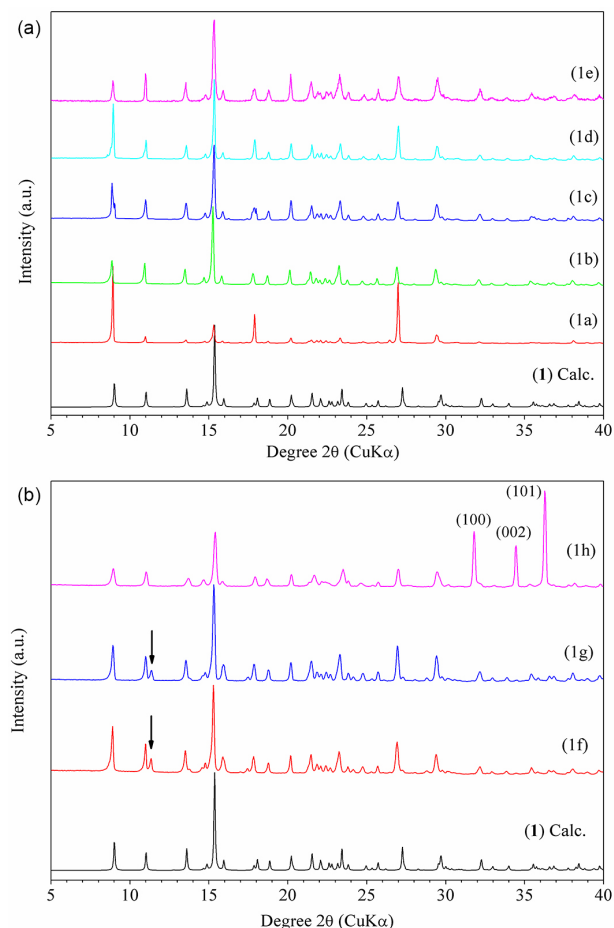


Figure 2. PXRD patterns for products (a) **1a-1e** and (b) **1f-1h**. For identification purposes, the calculated powder pattern of **1** obtained from the single-crystal X-ray diffraction data is also shown. The black arrows in the **1f-1g** PXRD patterns indicate Bragg peaks that do not match to crystal structure of **1**. Reflexions marked with the Miller index (100), (002) and (101) in the **1h** PXRD pattern indicate the presence of unreacted ZnO (ICDD crystal chart No. 36-1451). The X-ray diffraction pattern calculated from low-temperature crystal structure (150 K, see Table 1) is, as expected, slightly shifted (right direction) from the experimental ones performed at room temperature (298 K) for the products **1a-1h**.

All TG (thermogravimetry) curves (Figure S1, in the Supplementary Information (SI) section), even those ones of samples pointed out as pure by PXRD data, show an unexpected mass loss from 40 to 90 °C. This in common behavior is associated with loss of water absorbed by the samples due to ambient moisture, since no empty spaces in the crystal unit cell of **1** large enough to hold water molecule

was found using Mercury³¹ to display the percentage of void. After approximately 100 °C, the TG curves of the products obtained from methods A (**1a-1d**) and B (**1e**) are similar corroborating the PXRD analysis that pointed out to bulks constituted only by **1** as reactional product. On the other hand, the TG curves of the products obtained by method C (**1f-1g**) are slightly different from the previous ones due to the presence of the spurious phase indicated by the PXRD analysis. The TG curve of the product **1h** is, as expected, significantly different compared to the remaining ones due to the coexistence of ZnO and **1**. Therefore, the thermal analysis helps us to probe the purity of the bulk material of each synthesis corroborating that the products **1a-1d** and **1f-1g** are pure and impure, respectively. Taking this in account, the TG, DTG (differential thermogravimetry) and DTA (differential thermal analysis) curves of the product **1b** were arbitrarily chosen to be discussed in detail as a representative of **1**. In the temperature range from 40 to 90 °C, as mentioned above, it is observed a loss of 2.68% in weight in the TG curve of the product **1b**, which is attributed to the presence of moisture water. This event is also evident in the correspondent DTG and DTA curves. Thereafter, the TG curve reveals that compound **1** is stable up to 190 °C. Between 190-800 °C, the thermal decomposition occurs in two main steps as highlighted by correspondent DTG and DTA curves. It is first observed a weight loss of 22.42% from 205-390 °C, which corresponds to the loss of 1 mol of DMSO *per* formula unit (calcd. 24.21%). Then, a pyrolysis of the coordinated ligand occurs and finishes at 800 °C with a weight loss of 50.32% (calcd. 50.56%). The residue is characterized as ZnO (25.31%, calcd. 25.23%).

Since the compound **1** is present in the final synthesis products obtained in this study, we can notice that the infrared spectral data for the eight samples (Figure S2, in the SI section) are quite similar for the pure bulks (**1a-1e**) and comparable to the bulks with spurious phase coexistence (**1f-1h**). Some extra spectral differences are observed due to the sample hygroscopicity. The infrared spectrum of the product **1b** was also arbitrary chosen between the samples obtained by method A to be discussed in detail as representative of **1**. The spectrum of **1b** indicates the presence of a weak band in the region of 3000 cm⁻¹ (2914.44 cm⁻¹) attributed to C–H (sp³) stretching, a band near to 1440 cm⁻¹ (1440.83 cm⁻¹) attributed to C–H (sp³) bending, and a band near to 1030 cm⁻¹ (1028.06 cm⁻¹), characteristic of stretching of sulfoxide group. These bands indicate the presence of DMSO molecule in the structure. In addition, the presence of an intense doublet in the 3200 cm⁻¹ zone (3253.91 and 3136.25 cm⁻¹), which is attributed to $\nu(\text{N-H})$ symmetric and asymmetric of primary amines; and an intense band near to 1590 cm⁻¹ (1589.34 cm⁻¹),

indicates the protonation of amine group as confirmed by the single crystal X-ray structure determination of **1** (see below). The strong band in 1627.92 cm^{-1} can be attributed to C=O stretching and the presence of single band near to 1250 cm^{-1} (1251.80 cm^{-1}), attributed to carboxylic acid C–O stretching, indicates that this group is deprotonated. The broad band in the 3400 cm^{-1} region indicates that the sample present water of moisture, which is in agreement with the mass loss observed between $40\text{--}90\text{ }^{\circ}\text{C}$ in the TG curves.

Crystal structure analysis of [Zn(aip)(DMSO)] (**1**)

Based on the diffusion method using water and DMSO as the solvents (synthesis **1a**), we obtained appropriated single crystals of **1**. The single-crystal X-ray diffraction data show that **1** crystallizes in the monoclinic $P2_1/c$ space group, and its asymmetric unit contains one Zn^{II} ion, one disordered molecule of DMSO and one aip molecule (Figure 3a).

The ligand connects three metal centers through their carboxylates (monodentate mode) and via the nitrogen atom of the amine function. The Zn^{II} ions are in a tetrahedral distorted geometry, which extends the structure into a two-dimensional network, as discussed later (Figure 3b). Its molecular structure was studied with the Mogul software,³³ and the analysis indicates that all bond lengths and bond angles are consistent with those expected for well refined structures and similar fragments of deposited molecules in the Cambridge Structural Database (CSD).³⁴

From the topological viewpoint, this network can be simplified as a 6^3 uninodal honeycomb-type network (hcb net),³⁵ which forms parallel layers to the plane (100) (Figure 4a). The layers are stacked and form bilayers (layer A and layer B) connected by hydrogen bonds (Figure 4b) that involve the $\text{N1}\text{--H1}\cdots\text{O1}$ and $\text{N1}\text{--H2}\cdots\text{O3}$ systems (Table S1, in the SI section) and generate two

supramolecular synthons: $\text{R}_2^2(14)$ and $\text{R}_2^2(11)$,³⁶ respectively (Figure 4b). A bilayer with the intra-layer DMSO molecules is oriented in the same direction, and the inter-layer ones are oppositely (up vs. down) oriented (Figure 4b).

The DMSO-free bilayers (shortest interlayer distance (d_1)) extend along the [100] direction (longest interlayer distance (d_2)) with the DMSO methyl moieties interpenetrated in a zig-zag fashion (Figure 5). To calculate the distance among layers A, B and A' of **1**, we traced the planes through the Zn^{II} atoms of each layer; the A and B distance (d_1) is equal to 4.128 \AA , and the B and A' distance (d_2) is equal to 5.688 \AA (Figure 5).

Comparing compound **1** with Zn^{II} analogues

In this part, the structure of **1** is compared to some Zn^{II} 2D CPs reported in recent years^{25-27,37-39} that are coordinated to three μ^3 -aip ligands with a coordination sphere completed by an arbitrary ligand L. These CPs with general formula [Zn(aip)(L)] are called here as CPO-8-L analogues.

Compound **1** and the known CPO-8-L analogues have a 2D honeycomb-type structure, in which three μ^3 -aip ligands are coordinated to three metal ions by the carboxylate oxygen atoms (with a monodentate coordination mode) and nitrogen atom of the amine function. The structure forms a 22-membered metalomacrocyclic (Figure 3b), in which the linker L always faces out of the plane formed by the metals. The Zn–O and Zn–N distances for compound **1** and its analogues are shown in Table S3 (in the SI section).

As previously mentioned, the macrocycles extend along the [001] direction through covalent bonds and along [100] through intermolecular hydrogen bonds to form bilayers. Comparing the distances of the layers of **1** and its CPO-8-L analogues, we find that the distance between layers A and B (d_1) (Figure 5) is similar for all compounds (Table S2, in the SI section) because this space is spanned by

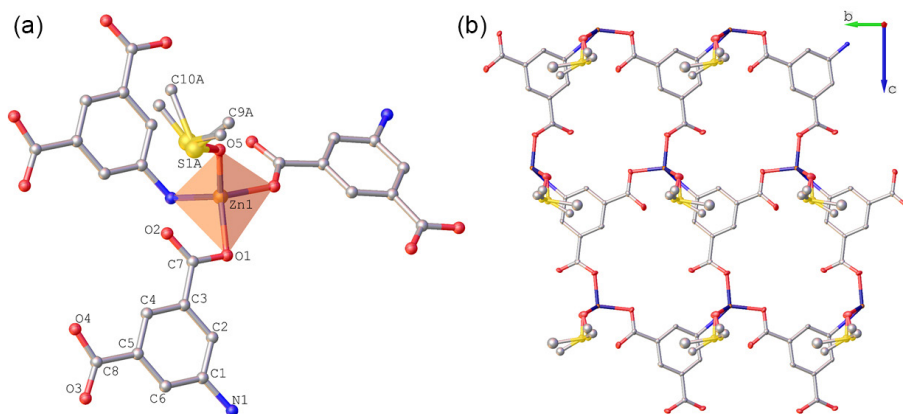


Figure 3. Ellipsoid representation of compound **1** with atomic labeling: (a) the asymmetric unit, tetrahedral environment of the metal and (b) two-dimensional network. The hydrogen atoms were omitted for clarity.

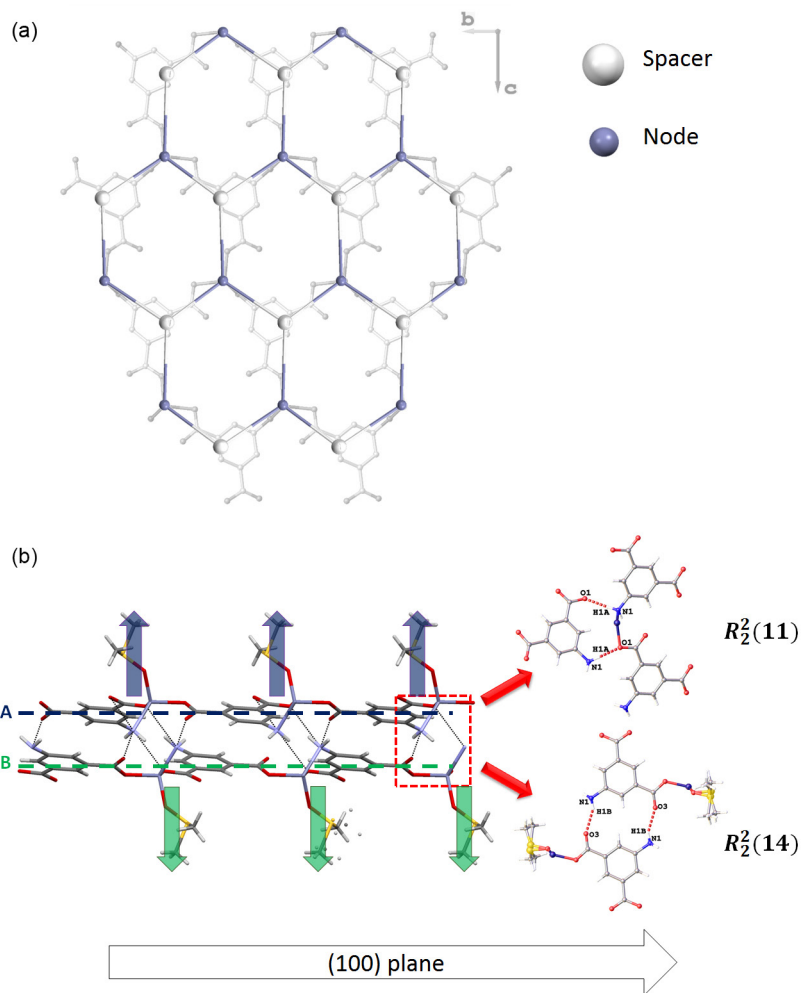


Figure 4. (a) Simplified view of the compound 1 showing the honeycomb-type network and (b) intermolecular hydrogen bonds (dashed lines) that connect layers A and B. The supramolecular synthons are highlighted and DMSO molecules are indicated with blue and green blue arrows (pointing upward and downward, respectively) to show the opposite directions to each layer.

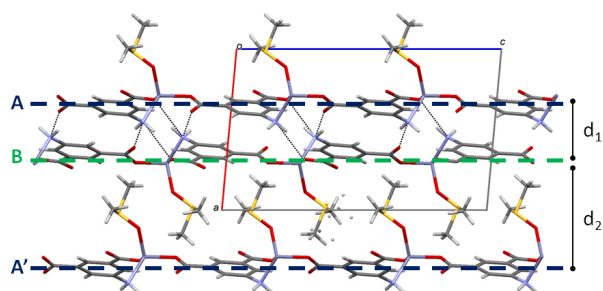


Figure 5. Shortest (d_1) and longest (d_2) interlayer distances for compound 1.

intermolecular hydrogen bonding, with identical magnitudes for all. However, the distances between layers B and A' (d_2) (Figure 5) vary according to the molecular volume of ligand L coordinated to the metal (Table S2, in the SI section).

Analyzing the individual ligand, we observe that the carboxylate groups can have similar or supplementary torsion angles (θ_1 and θ_2). When the carboxylate groups have similar torsional angles ($\theta_1 \approx \theta_2$),^{38,39} the aip ligand has

the same orientation throughout the network (orientation 1) (CPO-8-L1). However, when the carboxylates are twisted relative to one another ($\theta_2 \approx \theta_1 + 180^\circ$),^{25,26,37,39} as is the case of compound 1, the ligand aip has two distinct directions across the network (orientations 1 and 2) (CPO-8-L2) (Figure 6).

This difference is related to the presence of intermolecular hydrogen bonds³⁸ and coordination number of the metal center,³⁹ which are presented by the representatives of CPO-8-L1. The compound catena-((μ 3-5-aminoisophthalate)-(1*H*-imidazole-N3)-zinc hydrate) (CPO-8-IMDZ, IMDZ: imidazole)³⁸ has an imidazole molecule that occupies the L position. This ligand is responsible for the presence of an intermolecular hydrogen bond between the N–H group and the uncoordinated oxygen atom of the aip molecule (Figure 7). This hydrogen bond forces the torsion angles of the carboxylates to be similar. Because the compound catena-[(μ 3-5-aminoisophthalato)-(1,10-phenanthroline)-zinc(II)] (CPO-8-PHE, where PHE: phenanthroline)³⁹

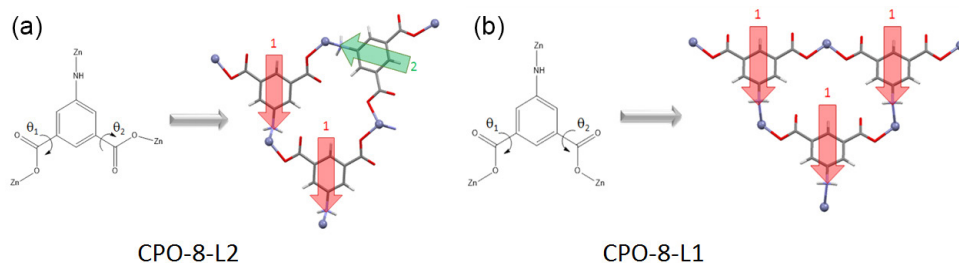


Figure 6. Effect of the torsion angle on the orientation of the ligand aip in the network for compound **1**, the (a) CPO-8-L2 analogues and (b) CPO-8-L1 analogues (CSD code: OBODOA).³⁸ The red and green arrows indicate orientations 1 and 2, respectively, of the aip molecule in the two-dimensional network.

has a phenanthroline molecule (a bidentate ligand) that occupies the L position, the metal center shows a coordination number of 5, unlike the other representative CPO-8-L, which affects the torsion of the carboxylates. Without these conditions, the compounds with Zn^{II} and aip behave similarly to compound **1**. The torsion angles of compound **1** and its analogues are provided in Table S4 (in the SI section).

Compound **1** and its CPO-8-L2 analogues have in common an intramolecular hydrogen bond type S(6)³⁶ (Figure 8a), which involves the nitrogen atom of the amino group (N1) and the uncoordinated oxygen atom (O2) ($d(D-A) = 3.057 \text{ \AA}$ for **1**). This interaction is not present in the CPO-8-L1 analogues (Figure 8b). This structural feature can be explained by the orientation of the ligands, as previously discussed. For the CPO-8-L2 analogues, the ligands with orientation 1 are not coplanar, permitting the connection between the oxygen atom O(2) and the

nitrogen atom N(1). The same is not true for the analogs of CPO-8-L1 because the ligands are coplanar and form parallel chains along the network.

Conclusions

The two-dimensional coordination polymer [Zn(aip)(DMSO)] with a honeycomb-type network was synthesized under different synthetic conditions, which proves the high thermodynamic and kinetic stability and invariance of this structure. This characteristic is of great interest because the identical product may be obtained at room temperature with minimum solvent use (e.g., mechanochemical method), which can be considered an appeal from the point of view of green chemistry.

Comparing compound **1** with the reported Zn^{II} analogues in the literature, we observe that the structure consists of three aip ligands that bridge three metal ions,

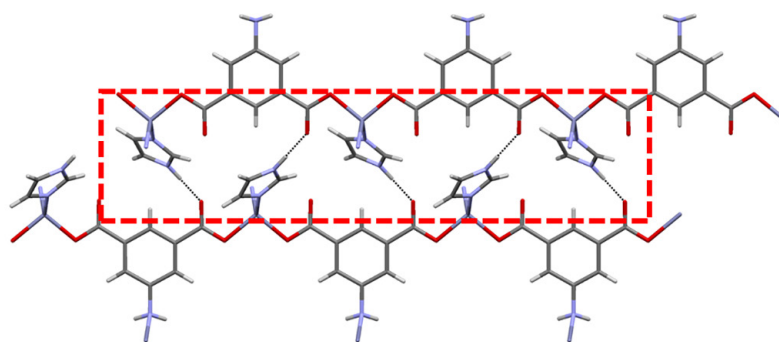


Figure 7. Intermolecular hydrogen bond (dashed line) between the N–H moiety of the imidazole molecule and the uncoordinated oxygen of the aip ligand, which directly affects the torsion angle of compound CPO-8-IMDZ.³⁸

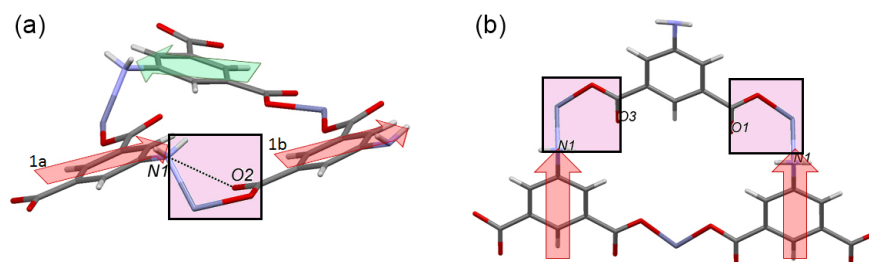


Figure 8. (a) Intramolecular hydrogen bond in **1** and the CPO-8-L2 analogues because of the non-coplanarity of the ligands with orientation 1 (red arrow), and (b) the absence of intramolecular hydrogen bond in the CPO-8-L1 analogues (CSD code: OBODOA).³⁸

and the DMSO molecule faces out of the plane formed by the metal ions. Hence, our results confirm the tendency of these metal-ligand combinations to form isostructural compounds with the general formula [Zn(aip)(L)].

Supplementary Information

CCDC-1448444 contains the supplementary crystallographic data for this paper. The data can be obtained free of charge from The Cambridge Crystallographic Data Centre at www.ccdc.cam.ac.uk/getstructures. CIF file, tables containing extra crystallographic data, extra PXRD patterns, thermal analysis curves and infrared spectra are available free of charge at <http://jbcs.sbq.org.br> as PDF file.

Acknowledgments

The authors thank FINEP (ref. 134/08), CNPq (308354/2012-5, 448723/2014-0 and 308162/2015-3), CAPES (AUXPE- PNPd 2347/2011), FAPEMIG (RED-00010-14, APQ-00273-14 and APQ-02486-14) for financial support. We also thank CNPq (A. C. Z. S., C. B. P. and A. C. D.) and FAPEMIG (I. M. L. R.) for research fellowships. This work is a collaboration research project of members of the Rede Mineira de Química (RQ-MG) supported by FAPEMIG (Project CEX RED-00010-14). The authors express sincere thanks to LabCri (UFMG) for the X-ray facilities.

References

- Raptopoulou, C. P.; Sanakis, Y.; Lazarou, K. N.; Georgopoulou, A. N.; Pissas, M.; Psycharis, V.; *Polyhedron* **2015**, *34*, 783.
- Tao, J.; Yin, X.; Jiang, Y.-B.; Huang, R.-B.; Zheng, L.-S.; *Inorg. Chem. Commun.* **2003**, *6*, 1171; Li, X.; Yuan, D.; Zhang, X.; Cao, R.; *J. Coord. Chem.* **2006**, *59*, 969; McManus, G. J.; Wang, Z.; Beauchamp, D. A.; Zaworotko, M. J.; *Chem. Commun.* **2007**, 5212; Liu, Y.-Y.; Jiang, Y.-Y.; Yang, J.; Liu, Y.-Y.; Ma, J.-F.; *CrystEngComm* **2011**, *13*, 6118; Ge, Y.; Li, N.-Y.; Ji, X.-Y.; Wang, J.-F.; Liu, D.; Tang, X.-Y.; *CrystEngComm* **2014**, *16*, 6621; Wang, X.; Sui, F.; Lin, H.; Zhang, J.; Liu, G.; *Cryst. Growth Des.* **2014**, *14*, 3438.
- Tao, J.; Yin, X.; Jiang, Y. B.; *Inorg. Chem. Commun.* **2003**, *6*, 1171.
- Fan, J.; Xiao, T.; Zheng, S.-R.; Cai, S.-L.; Zhang, W.-G.; *Inorg. Chem. Commun.* **2011**, *14*, 1156.
- Kuppler, R. J.; Timmons, D. J.; Fang, Q.-R.; Li, J.-R.; Makal, T. A.; Young, M. D.; Yuan, D.; Zhao, D.; Zhuang, W.; Zhou, H.-C.; *Coord. Chem. Rev.* **2009**, *253*, 3042; Furukawa, H.; Cordova, K. E.; O'Keeffe, M.; Yaghi, O. M.; *Science* **2013**, *341*, 1230444.
- Eddaoudi, M.; Sava, D. F.; Eubank, J. F.; Adil, K.; Guillemin, V.; *Chem. Soc. Rev.* **2015**, *44*, 228.
- Yeung, H. H.-M.; Cheetham, A. K.; *Dalton Trans.* **2014**, *43*, 95.
- Bohnsack, A. M.; Ibarra, I. A.; Bakhmutov, V. I.; Lynch, V. M.; Humphrey, S. M.; *J. Am. Chem. Soc.* **2013**, *135*, 16038; Wang, S. N.; Xiong, S. S.; Wang, Z. Y.; Du, J. F.; *Chem. Eur. J.* **2011**, *17*, 8630.
- Xue, M.; Zhu, G. S.; Zhang, Y. J.; Fang, Q. R.; Hewitt, I. J.; Qiu, S. L.; *Cryst. Growth Des.* **2008**, *8*, 427; O'Keeffe, M.; Peskov, M. A.; Ramsdell, S. J.; Yaghi, O. M.; *Acc. Chem. Res.* **2008**, *41*, 1782.
- Reichel, F.; Clegg, J. K.; Gloe, K.; Weigand, J. J.; Reynolds, J. K.; Li, C.-G.; Aldrich-Wright, J. R.; Kepert, C. J.; Lindoy, L. F.; Yao, H.-C.; Li, F.; *Inorg. Chem.* **2014**, *53*, 688.
- Carlucci, L.; Ciani, G.; García-Ruiz, J. M.; Moret, M.; Proserpio, D. M.; Rizzato, S.; *Cryst. Growth Des.* **2009**, *9*, 5024.
- Cheng, L.; Zhang, L. M.; Gou, S. H.; Cao, Q. N.; Wang, J. Q.; Fang, L.; *CrystEngComm* **2012**, *14*, 4437; Yu, F.; Li, B.; *CrystEngComm* **2011**, *13*, 7025; Gao, Y.; Cao, J.; Song, Y.; Zhang, G.; Wang, Y.; Liu, Z.; *CrystEngComm* **2013**, *15*, 8522; Mahmoudi, A.; Dehghanpour, S.; Gholamrezazadeh, C.; Jahanbakhshyan, M.; Mahmoudikhani, A. H.; Attari, N.; *Polyhedron* **2012**, *42*, 265.
- Pan, L.; Frydel, T.; Sander, M. B.; Huang, X.; Li, J.; *Inorg. Chem.* **2001**, *40*, 1271; Campos, N. R.; Ribeiro, M. A.; Oliveira, W. X. C.; Reis, D. O.; Stumpf, H. O.; Doriguetto, A. C.; Machado, F. C.; Pinheiro, C. B.; Lloret, F.; Julve, M.; Cano, J.; Marinho, M. V.; *Dalton Trans.* **2016**, *45*, 172; Barros, W. P.; da Silva, B. C.; Reis, N. V.; Pereira, C. L. M.; Doriguetto, A. C.; Cano, J.; Pirota, K. R.; Pedroso, E. F.; Julve, M.; Stumpf, H. O.; *Dalton Trans.* **2014**, *43*, 14586; Pereira, C. L. M.; Pedroso, E. F.; Doriguetto, A. C.; Ellena, J. A.; Boubekour, K.; Filali, Y.; Journaux, Y.; Novak, M. A.; Stumpf, H. O.; *Dalton Trans.* **2011**, *40*, 756.
- Rosa, I. M. L.; Costa, M. C. S.; Vitto, B. S.; Amorim, L.; Correa, C. C.; Pinheiro, C. B.; Doriguetto, A. C.; *Cryst. Growth Des.* **2016**, *16*, 1606.
- Cao, T.; Peng, Y.; Liu, T.; Wang, S.; Dou, J.; Li, Y.; Zhou, C.; Li, D.; Bai, J.; *CrystEngComm* **2014**, *16*, 10658; Fang, Z. L.; He, J. G.; Zhang, Q. S.; Zhang, Q. K.; Wu, X. Y.; Yu, R. M.; Lu, C. Z.; *Inorg. Chem.* **2011**, *50*, 11403; Li, Y. W.; Ma, H.; Chen, Y. Q.; He, K. H.; Li, Z. X.; Bu, X. H.; *Cryst. Growth Des.* **2012**, *12*, 189.
- Zhang, W.-Q.; Zhang, W.-Y.; Wang, R.-D.; Ren, C.-Y.; Li, Q.-Q.; Fan, Y.-P.; Liu, B.; Liu, P.; Wang, Y. Y.; *Cryst. Growth Des.* **2017**, *17*, 517.
- Yang, J.-X.; Zhang, X.; Cheng, J.-K.; Zhang, J.; Yao, Y.-G.; *Cryst. Growth Des.* **2012**, *12*, 333.
- Zheng, Y.-Q.; Xie, H.-Z.; *J. Solid State Chem.* **2004**, *177*, 1352; Dietzel, P. D. C.; Morita, Y.; Blom, R.; Fjellvåg, H.; *Angew.*

- Chem., Int. Ed.* **2005**, *44*, 6354; Dietzel, P. D. C.; Johnsen, R. E.; Blom, R.; Fjellvåg, H.; *Chem. - Eur. J.* **2008**, *14*, 2389.
19. Yeung, H. H.-M.; Cheetham, A. K.; *Dalton Trans.* **2014**, *43*, 95; Eigen, M.; *Pure Appl. Chem.* **1963**, *6*, 97.
20. Deng, Q.-J.; Wu, M.-C.; Liu, Z.-T.; Zeng, M.-H.; Huang, J.-Y.; Liang, H.; *J. Mol. Struct.* **2008**, *876*, 162.
21. Hu, Y.; Zhang, W.; Zhang, X.; Zhang, Z.; Li, Y.; Bai, J.; *Inorg. Chem. Commun.* **2009**, *12*, 166.
22. Sarma, D.; Ramanujachary, K. V.; Lofland, S. E.; Magdaleno, T.; Natarajan, S.; *Inorg. Chem.* **2009**, *48*, 11660.
23. Yuan, W.; Liu, T.; Guo, Z.; Li, H.; Cao, R.; *J. Mol. Struct.* **2010**, *965*, 82.
24. Wu, C.-D.; Lu, C.-Z.; Yang, W.-B.; Zhuang, H.-H.; Huang, J.-S.; *Inorg. Chem.* **2002**, *41*, 3302.
25. Kongshaug, K. O.; Fjellvåg, H.; *Inorg. Chem.* **2006**, *45*, 2424.
26. Yang, S.-Y.; Yuan, H.-B.; Xu, X.-B.; Huang, R.-B.; *Inorg. Chim. Acta* **2013**, *403*, 53.
27. Zhang, J. J.; Wojtas, L.; Larsen, R. W.; Eddaoudi, M.; Zaworotko, M. J.; *J. Am. Chem. Soc.* **2009**, *121*, 17040; Foster, P. M.; Stock, N.; Cheetham, A. K.; *Angew. Chem., Int. Ed.* **2005**, *44*, 7608.
28. Agilent; *CrysAlis Pro*; Agilent Technologies Ltd, Yarnton, Oxfordshire, UK, 2006.
29. Altamore, A.; Cascarano, G.; Giacobozzo, C.; Guagliardi, A.; Burla, M. C.; Polidori, G.; Camalli, M.; *J. Appl. Crystallogr.* **1994**, *27*, 435.
30. Sheldrick, G. M.; *Acta Crystallogr., Sect. C: Struct. Chem.* **2015**, *71*, 3.
31. Macrae, C. F.; Edgington, P. R.; McCabe, P.; Pidcock, E.; Shields, G. P.; Taylor, R.; Towler, M.; van de Streek, J.; *J. Appl. Crystallogr.* **2006**, *39*, 453.
32. Bisht, K. K.; Chaudhari, J.; Suresh, E.; *Polyhedron* **2015**, *87*, 71; Strobridge, F. C.; Judas, N.; Friscic, T.; *CrystEngComm* **2010**, *12*, 2409; Rad, M.; Dehghanpour, S.; *RSC Adv.* **2016**, *6*, 61784.
33. Bruno, I. J.; Cole, J. C.; Kessler, M.; Luo, J.; Motherwell, W. S.; Purkis, L. H.; Smith, B. R.; Taylor, R.; Cooper, R. I.; Harris, S. E.; *J. Chem. Inf. Comput. Sci.* **2004**, *44*, 2133.
34. Allen, F. H.; *Acta Crystallogr., Sect. B: Struct. Sci.* **2002**, *58*, 380.
35. Blatov, V. A.; *TOPOS*; Samara State University: Russia, 2004.
36. Bernstein, J.; Davis, R. E.; Shimoni, L.; Chang, N.; *Angew. Chem., Int. Ed.* **1995**, *34*, 1555.
37. Zhang, K.-L.; Qiao, N.; Gao, H.-Y.; Zhou, F.; Zhang, M.; *Polyhedron* **2007**, *26*, 2461.
38. Kuai, H.-W.; Cheng, X.-C.; *Acta Crystallogr., Sect. E: Crystallogr. Commun.* **2011**, *67*, m1835.
39. Wang, J.-J.; Bao, Q.-L.; Chen, J.-X.; *J. Coord. Chem.* **2013**, *66*, 2578.

Submitted: November 24, 2016

Published online: March 21, 2017